Yuzuncu Yil University
Journal of the Institute of Natural & Applied Sciences
https://dergipark.org.tr/en/pub/yyufbed

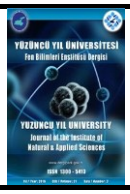

Research Article

Computational Investigation of Ternary Borides $Fe_3Al_2B_2$, $Ru_3Al_2B_2$, and $Os_3Al_2B_2$: Structural, Mechanical, and Phonon Properties

Sibel ÖZDOĞRU ŞENEL[*1], Engin ATEŞER[1,2], Hacı ÖZIŞIK[1,2], Engin DELİGÖZ[1,2]

[1]Aksaray University, Graduate School of Natural and Applied Sciences, Physics Department, 68100, Aksaray, Türkiye
[2]Aksaray University, Faculty of Arts and Sciences, Physics Department, 68100, Aksaray, Türkiye
*Corresponding author e-mail: sibelozdogru@hotmail.com

Abstract: An investigation has been conducted into the structural, mechanical, electronic, vibrational and thermal properties of $Fe_3Al_2B_2$, $Ru_3Al_2B_2$, and $Os_3Al_2B_2$ with the utilization of first-principles density functional theory (DFT) calculations. The optimized lattice parameters of $Fe_3Al_2B_2$ demonstrate a high degree of congruence with experimental data, thereby validating the efficacy of the utilized approach. The negative formation energies indicate the thermodynamic stability of all compounds while $Fe_3Al_2B_2$ has the highest structural stability. Mechanical analysis reveals that $Os_3Al_2B_2$ has the highest bulk modulus, while $Fe_3Al_2B_2$ possesses the highest shear modulus. Anisotropy mechanical calculations have confirmed that $Os_3Al_2B_2$ exhibits the strongest anisotropic behavior. Electronic band structure analysis showed that all compounds have metallic nature. Phonon dispersion calculations have been used to confirm the dynamical stability of $Fe_3Al_2B_2$ and $Ru_3Al_2B_2$, while $Os_3Al_2B_2$ has been shown to possess negative phonon modes, thus indicating potential instability. These findings indicate that $Fe_3Al_2B_2$ is the most mechanically and thermally stable compound and thus suitable for high strength applications, while the significant anisotropy of $Os_3Al_2B_2$ makes it ideal for applications requiring directional mechanical properties.

Keywords: Ab initio, $Fe_3Al_2B_2$, $Os_3Al_2B_2$, $Ru_3Al_2B_2$, Ternary Borides

$Fe_3Al_2B_2$, $Ru_3Al_2B_2$ ve $Os_3Al_2B_2$Üçlü Borürlerin Kuramsal İncelenmesi: Yapısal, Mekanik ve Fonon Özellikleri

Öz: Bu çalışmada $Fe_3Al_2B_2$, $Ru_3Al_2B_2$ ve $Os_3Al_2B_2$ bileşiklerinin yapısal, mekanik, elektronik, titreşimsel ve termal özellikleri yoğunluk fonksiyonel teorisine (DFT) dayalı hesaplamalar kullanılarak araştırılmıştır. $Fe_3Al_2B_2$'nin hesaplanan optimize örgü parametreleri deneysel verilerle gösterdiği iyi derecede uyumluluk kullanılan yaklaşımın etkinliğini ortaya koymaktadır. Belirlenen oluşum enerjilerinin negatif olması tüm bileşiklerin termodinamik kararlılığını gösterirken, $Fe_3Al_2B_2$ en yüksek yapısal kararlılığa sahiptir. Mekanik analizler $Os_3Al_2B_2$'nin en yüksek bulk modülüne, $Fe_3Al_2B_2$'nin ise en yüksek kayma modülüne sahip olduğunu ortaya koymaktadır. Mekanik anizotropi hesaplamaları $Os_3Al_2B_2$'nin en güçlü anizotropik davranışı sergilediğini doğrulamıştır. Elektronik band yapılarının analizi sonucu tüm bileşiklerin metalik doğaya sahip olduğunu görülmüştür. Fonon dağınımlarından $Fe_3Al_2B_2$ ve $Ru_3Al_2B_2$'nin dinamik kararlılıklar doğrulanmış olup, $Os_3Al_2B_2$'de görülen negatif fonon modları bileşiğin potansiyel kararsızlığa işaret etmektedir. Bu bulgular, $Fe_3Al_2B_2$'nin mekanik ve termal olarak en kararlı bileşik olduğunu ve bu nedenle yüksek mukavemetli uygulamalar için uygun olduğunu gösterirken, $Os_3Al_2B_2$'nin yüksek anizotropisi onu yönelime bağlı mekanik özellikler gerektiren uygulamalar için ideal hale getirmektedir.

Anahtar Kelimeler: Ab initio, $Fe_3Al_2B_2$, $Os_3Al_2B_2$, $Ru_3Al_2B_2$, Üçlü Borürler

Received: 28.03.2025
Accepted: 28.04.2025

How to cite: Özdoğru Şenel, S., Ateşer, E., Özışık, H., & Deligöz, E. (2025). Computational investigation of ternary borides Fe3Al2B2, Ru3Al2B2, and Os3Al2B2: Structural, mechanical, and phonon properties. *Yuzuncu Yil University Journal of the Institute of Natural and Applied Sciences*, *30*(2), 499-511. https://doi.org/10.53433/yyufbed.1667463

1. Introduction

Boron and boron-containing compounds have a significant role in technological applications (Fahrenholtz et al., 2007; Ade & Hillebrecht, 2015; Eroğlu et al., 2023). Transition metal borides (TMBs) have attracted considerable interest in both fundamental scientific investigations and practical applications because of their distinctive physical properties (Eremets et al., 2001; Eroğlu et al., 2023). Borides have several interesting properties, such as complex chemical structures, high chemical, thermal and mechanical stability, and the presence of both superconductivity and magnetism (Corral&Loehman, 2008). As a consequence of these properties, it is unsurprising that borides have found practical applications in a variety of technological domains (Lu et al., 2017; Zhang et al., 2018; Zhang et al., 2019a; 2019b). Metal borides have industrial applications, such as coatings for cutting tools and wear resistance, and are considered to be promising materials for applications such as the production of permanent magnets, primary battery electrodes and reinforcing materials in composites (Herbstet al., 1991; Opeka et al., 1999; Martini et al., 2004; Panda & Chandran, 2006; Licht et al., 2007; Yu & Licht, 2008; Blum et al., 2008; Zapata-Solvas et al., 2013). For example, it is known that compounds such as Mo_2FeB_2 and Mo_2NiB_2 can be used in the manufacture of machine components with high corrosion resistance (Takagi, 2006). Ternary borides offer greater design flexibility, allowing many structural and performance properties to be explored, and they also stand out as superhard materials (Huang et al., 2025). The wide range of applications of borides makes research on new borides important and attractive, and the literature contains a number of relevant studies (Cheng et al., 2014; Ali et al., 2017; Kota et al., 2018; Feng et al., 2018; Ali et al., 2020). However, further research on ternary borides is needed.

$Fe_3Al_2B_2$, an important member of the ternary boride family, was first synthesized in the monoclinic structure by Hirt et al. (2018). The structural motifs of binary and ternary transition metal borides are reported to be exhibited by $Fe_3Al_2B_2$ (Hirt et al., 2018). However, detailed theoretical studies on this compound have remained limited. A comprehensive study using ab initio calculations can provide essential insights into the electronic, mechanical and phonon properties of the material. In this study, besides $Fe_3Al_2B_2$, the compounds $Ru_3Al_2B_2$ and $Os_3Al_2B_2$ were also considered and their structural, electronic, mechanical and phonon properties are investigated in detail by ab initio methods. This study aims to provide a comprehensive theoretical basis for the potential applications of these compounds.

2. Materials and Methods

The structural, electronic, mechanical and phonon properties are investigated using density functional theory (DFT) implemented in the VASP code (Kresse & Furthmüller, 1996a; 1996b; Kresse & Joubert, 1999). The Perdew-Burke-Ernzerhof (PBE) functional with the generalized gradient approximation (GGA) (Perdew et al., 1996) was used to describe the exchange-correlation interactions. The configurations of the valence electrons are Fe: $3d^7\ 4s^1$, Ru: $3d^7\ 4s^1$: $4p^6\ 4d^7\ 5s^1$, Os: $5d^7\ 6s^1$, Al: $3s^2\ 3p^1$ and B: $2s^2\ 2p^1$, respectively. It was established that the systems were fully relaxed, with energy convergence reaching a minimum of 10^{-5} eV. The optimized structures were obtained with a maximum force per atom of less than 0.001 eV $Å^{-1}$, and a plane wave cut-off energy of 400 eV was utilized for the titled compounds. An 8×15×4 k-point mesh generated using the Monkhorst-Pack scheme (Monkhorst & Pack, 1976) was used in the first irreducible Brillouin zone for structural, electronic and mechanical properties calculations.

The elastic constants were obtained through the stress-strain method (Le page & Saxe, 2002) implemented in the VASP code. The interatomic force constant for phonon calculations was calculated in the PHONOPY code using VASP-DFPT in the 2x3x1 supercell (Togo et al., 2023; Togo, 2023) with the 4x4x4 k-point mesh.

3. Results and Discussion

3.1. Structural properties

The obtained structural parameters of $Fe_3Al_2B_2$, $Ru_3Al_2B_2$, and $Os_3Al_2B_2$ ternary borides that have crystallized in the monoclinic structure (space group *P*2/m, space group number: 10) are presented in Table 1, with the experimental value (Hirt et al., 2018) . Furthermore, to provide a more comprehensive perspective, the crystal structures of $Fe_3Al_2B_2$, $Ru_3Al_2B_2$, and $Os_3Al_2B_2$ are shown in Figure 1.

The lattice parameters calculated for $Fe_3Al_2B_2$ compound are in good agreement with the experimental result (Hirt et al., 2018). The structural parameter for $Ru_3Al_2B_2$ and $Os_3Al_2B_2$ compounds and the formation energies for all compounds were calculated for the first time in this study. Similar lattice parameters were observed for $Ru_3Al_2B_2$ and $Os_3Al_2B_2$, but the volume (V_0) of the compounds containing Ru and Os seems to be larger compared to the compound containing Fe. This can be explained by the fact that Ru and Os have larger atomic radii. All borides have negative formation energy, indicating that they are thermodynamically stable. It can be noted that the formation energy value calculated for $Fe_3Al_2B_2$ is the lowest at -0.6224 eV/p.a, indicating that this compound is more stable than $Ru_3Al_2B_2$ (-0.4929 eV/p.a) and $Os_3Al_2B_2$ (-0.2264 eV/p.a).

Table 1. The calculated structural parameters (a, b and c in Å; β in degree), c/a ratio, volumes (V_0, Å^3/f.u.) and formation energy (ΔH_f , eV/p.a.)

Material	*a*	*b*	*c*	*β*	*c/a*	V_0	ΔH_f	Refs.
$Fe_3Al_2B_2$	5.7107	2.7764	8.7269	98.6	1.528	136.8	-0.6224	Present
	5.7236	2.8567	8.7229	98.57	1.524	141.03		Exp. (Hirt et al., 2018)
$Ru_3Al_2B_2$	5.9741	2.9165	9.2652	98.7	1.551	159.6	-0.4929	Present
$Os_3Al_2B_2$	5.9779	2.9185	9.2733	98.7	1.551	159.9	-0.2264	Present

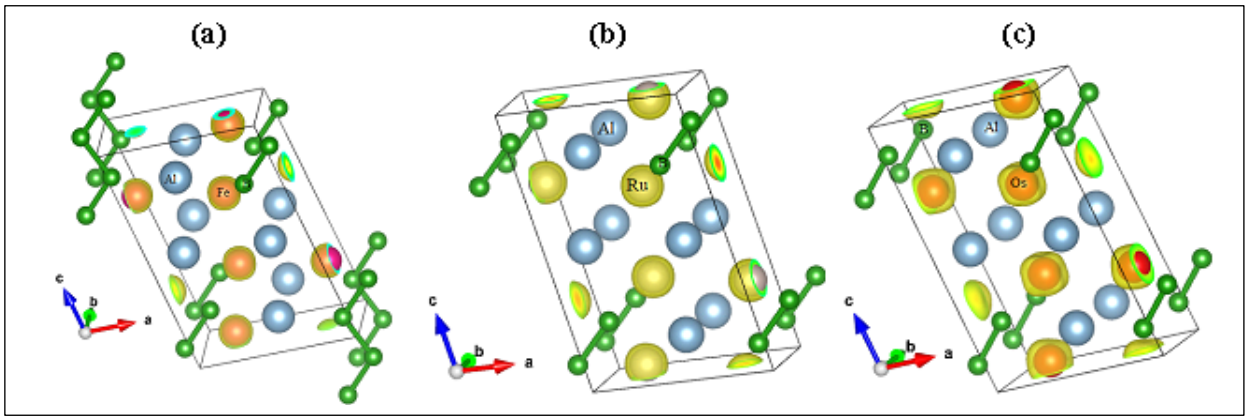

Figure 1. Crystal structure views; (a) $Fe_3Al_2B_2$, (b) $Ru_3Al_2B_2$ and (c) $Os_3Al_2B_2$.

3.2. Mechanical properties

The elastic constants of $Fe_3Al_2B_2$, $Ru_3Al_2B_2$, and $Os_3Al_2B_2$ compounds, presented in Table 2, provide insight into their mechanical stability, rigidity, and anisotropic behavior. Unfortunately, experimental and theoretical data are not available to check our results. In the case of a monoclinic crystal, there are thirteen unique elastic constants; C_{ii} (i=1,2,3,4,5,6,), C_{1j} (j=2,3,5), C_{23}, C_{25}, C_{35}, and C_{46}.

Table 2. The calculated elastic constants (C_{ij} in GPa)

Material	C_{11}	C_{22}	C_{33}	C_{44}	C_{55}	C_{66}	C_{12}	C_{13}	C_{15}	C_{23}	C_{25}	C_{35}	C_{46}
$Fe_3Al_2B_2$	337.5	378.0	371.8	129.1	125.3	132.8	126.2	52.5	22.9	114.1	-3.5	0.3	5.6
$Ru_3Al_2B_2$	352.4	456.7	371.1	99.4	90.1	109.5	129.6	178.5	11.4	135.4	-13.7	-0.9	-1.9
$Os_3Al_2B_2$	339.9	507.5	369.3	73.0	99.0	61.4	141.1	220.7	13.0	176.7	-6.8	-4.6	43.4

The mechanical stability for a monoclinic structure, requires the following Born criteria (Ozisik et al., 2011; Mouhat & Coudert, 2014) to be satisfied:

$$C_{ii}\,(i=1,2,3,4,5,6) > 0, \tag{1}$$

$$[C_{11} + C_{22} + C_{33} + 2(C_{12} + C_{13} + C_{23})] > 0,\ C_{33}C_{55} - C_{35}^2 > 0,\ C_{44}C_{66} - C_{46}^2 > 0 \tag{2}$$

$$C_{22} + C_{33} - 2C_{23} > 0,\ \ C_{22}(C_{33}C_{55} - C_{35}^2) + 2C_{23}C_{25}C_{35} - (C_{23}^2)C_{55} - (C_{25}^2)C_{33} > 0 \tag{3}$$

$$\begin{aligned} &2[C_{15}C_{25}(C_{33}C_{12} - C_{13}C_{23}) + C_{15}C_{35}(C_{22}C_{13} - C_{12}C_{23}) + C_{25}C_{35}(C_{11}C_{23} - C_{12}C_{13})] - \\ &[C_{15}C_{15}(C_{22}C_{33} - C_{23}^2) + C_{25}C_{25}(C_{11}C_{33} - C_{13}^2) + C_{35}C_{35}(C_{11}C_{22} - C_{12}^2)] + C_{55}g > 0 \end{aligned} \tag{4}$$

The elastic constants of the compounds meet these criteria, confirming their mechanical stability.

The constants C_{11}, C_{22} and C_{33} indicate of uniaxial stress with incompressible property in the *x*-, *y*- and *z*-directions, respectively. $Os_3Al_2B_2$ compound exhibits the highest C_{22} value, followed by $Ru_3Al_2B_2$ and $Fe_3Al_2B_2$, indicating that $Os_3Al_2B_2$ has the largest stiffness along the y-axis. In contrast, C_{33} values are relatively similar for all compounds, suggesting comparable compressibility along the z-axis.

As can be seen in Table 2, $Fe_3Al_2B_2$ exhibits the highest values of C_{44}, C_{55}, and C_{66} among the considered compounds. These elastic constants represent the shear moduli on the (100), (010), and (001) crystal planes, respectively (Ozisik et al., 2016). Therefore, $Fe_3Al_2B_2$ compound possesses the strongest anti-shearing ability on these planes, making it the least prone to shear-related deformation.

Using the calculated elastic constants, the bulk modulus B and shear modulus G can be estimated using the following equations according to the Voigt-Reuss-Hill (VRH) approach (Reuss, 1929; Hill, 1952; Voigt, 1966):

$$B_V = (1/9)\,[C_{11} + C_{22} + C_{33} + 2(C_{12} + C_{13} + C_{23})] \tag{5}$$

$$\begin{aligned} B_R = \Omega\,[&a\,(C_{11} + C_{22} - 2C_{12}) + b\,(2C_{12} - 2C_{11} - C_{23}) + c\,(C_{15} - 2C_{25}) + d\,(2C_{12} + 2C_{23} \\ &- C_{13} - 2C_{22}) + 2e\,(C_{25} - C_{15}) + f]^{-1} \end{aligned} \tag{6}$$

$$G_V = (1/15)\,[C_{11} + C_{22} + C_{33} + 3(C_{44} + C_{55} + C_{66}) - (C_{12} + C_{13} + C_{23})] \tag{7}$$

$$\begin{aligned} G_R = 15\,\{4[&a\,(C_{11} + C_{22} + C_{33}) + b\,(C_{11} - C_{12} - C_{23}) + c\,(C_{15} + C_{25}) + d\,(C_{22} - C_{12} - C_{23} \\ &- C_{13}) + e\,(C_{15} - C_{25}) + f] / \Omega + 3\,[g / \Omega + (C_{44} + C_{66}) / (C_{44}C_{66} - C_{46}^2)]\}^{-1} \end{aligned} \tag{8}$$

$$\begin{aligned} &a = C_{33}C_{55} - C_{35}^2,\ b = C_{23}C_{55} - C_{25}C_{35},\ c = C_{13}C_{35} - C_{15}C_{33},\ d = C_{13}C_{55} - C_{15}C_{35}, \\ &e = C_{13}C_{25} - C_{15}C_{23},\ f = C_{11}\,(C_{22}C_{55} - C_{25}^2) - C_{12}(C_{12}C_{55} - C_{15}C_{25}) + C_{15}(C_{12}C_{25} - C_{15}C_{25}) \\ &+ C_{25}(C_{23}C_{35} - C_{25}C_{33}),\ g = C_{11}C_{22}C_{33} - C_{11}C_{23}^2 - C_{22}C_{13}^2 - C_{33}C_{12}^2 + 2C_{12}C_{13}C_{23}, \\ &\Omega = 2[C_{15}C_{25}(C_{33}C_{12} - C_{13}C_{23}) + C_{15}C_{35}(C_{22}C_{13} - C_{12}C_{23}) + C_{25}C_{35}(C_{11}C_{23} - C_{12}C_{13})] - \\ &[C_{15}^2(C_{22}C_{33} - C_{23}^2) + C_{25}^2(C_{11}C_{33} - C_{13}^2) + C_{35}^2\,(C_{11}C_{22} - C_{12}^2)] + gC_{55} \end{aligned} \tag{9}$$

$$B = (B_V + B_R)/2 \ , \ G = (G_V + G_R)/2 \tag{10}$$

The Young's modulus E and Poisson's ratio ν are obtained from the following equations:

$$E = 9BG/(3B+G), \ \nu = (3B-2G)/[2(3B+G)]. \tag{11}$$

The calculated values for bulk modulus, shear modulus, Young's modulus, Pugh ratio, and Poisson's ratio are presented in Table 3.

Bulk modulus and shear modulus describe the resistance of a crystal to volume and shape changes, respectively (Ozisik et al., 2011). The calculated bulk moduli are $Os_3Al_2B_2$> $Ru_3Al_2B_2$ > $Fe_3Al_2B_2$. This indicates that $Os_3Al_2B_2$ has the highest resistance to compression. However, the shear modulus (G) shows an opposite variation with the bulk modulus in $Fe_3Al_2B_2$ > $Ru_3Al_2B_2$ > $Os_3Al_2B_2$. A higher modulus of shear usually means stronger covalent bonding and improved stiffness against shear forces. Young's modulus measures the stiffness of a material and its resistance to uniaxial elastic deformation. Among the three compounds, $Fe_3Al_2B_2$ exhibits the highest Young's modulus. This indicates that $Fe_3Al_2B_2$ has the greatest resistance to elastic deformation and is the hardest among the studied borides. $Os_3Al_2B_2$ has a higher flexibility with a lower Young's modulus. The results presented in Table 3 reveal that the bulk modulus consistently increase with the increasing atomic number of the transition metal, while the shear and Young modulus demonstrate a decrease.

Table 3. The calculated polycrystalline moduli (bulk *(B)*, Shear *(G)*, and Young's *(E)* in GPa), Pugh ratio (B/G), G/B ratio and Poisson's ratio *(ν)*

Material	B	G	E	B/G	G/B	ν
$Fe_3Al_2B_2$	207.822	122.479	307.107	1.697	0.589	0.254
$Ru_3Al_2B_2$	229.305	106.531	276.738	2.152	0.464	0.299
$Os_3Al_2B_2$	253.074	76.218	207.793	3.320	0.301	0.363

The Pugh ratio (B/G) (Pugh, 1954) is a useful indicator of the brittleness or ductility of a material. A B/G ratio above 1.75 indicates ductile behavior, while values below 1.75 indicate brittle behavior. The values calculated for ternary borides indicate that $Fe_3Al_2B_2$ is brittle but close to the brittle-ductile threshold. $Ru_3Al_2B_2$ is ductile, and $Os_3Al_2B_2$ exhibits highly ductile behavior. It should be noted that as the atomic number of transition metals increases, the ductile behavior of the compounds also increases.

Typically, covalent materials exhibit a Poisson's ratio of around 0.1, while ionic materials have a Poisson's ratio close to 0.25 (Ozisik et al., 2010). For the studied compounds, the calculated Poisson's ratio values suggest that atomic bonding is predominantly ionic in nature. Additionally, Poisson's ratio provides insight into the characteristics of bonding forces, where central forces have a theoretical lower limit of 0.25 and an upper limit of 0.5. The observed values indicate that central forces play a significant role in these materials. Furthermore, the G/B ratio, which is approximately 1.1 for covalent materials and 0.8 for ionic materials, further supports the predominance of ionic bonding in these compounds (see Table 3). $Os_3Al_2B_2$ compound has the highest Poisson's ratio value, confirming that it is the most ductile material. Two important thermodynamic parameters, the velocity of sound and Debye temperature, were calculated using the equations provided in Refs. (Anderson, 1963; Schreiber et al., 1975; Johnston et al., 1996). The calculated Debye temperatures and sound velocities are given in Table 4.

Table 4. The calculated longitudinal, transverse, and average sound velocities (V_l, V_t and V_m in m/s) and Debye temperature (θ_D in K), bulk and shear anisotropy (A_B and A_G in %) and universal anisotropic index (A^U)

Material	V_l	V_t	V_m	θ_D	A_B	A_G	A^U
$Fe_3Al_2B_2$	7930	4556	5060	704.6	0.13	1.07	0.11
$Ru_3Al_2B_2$	6870	3680	4110	543.3	0.17	2.22	0.23
$Os_3Al_2B_2$	5206	2413	2718	356.3	0.60	20.82	2.64

Higher Debye temperature means higher thermal conductivity, which implies stronger atomic interactions and higher phonon frequencies. Therefore, $Fe_3Al_2B_2$ is expected to have greater thermal conductivity, while $Os_3Al_2B_2$ has the lowest thermal conductivity. Moreover, $Os_3Al_2B_2$ has the lowest sound velocities, indicating its higher ductility and less resistance to deformation.
Elastic anisotropy is vital in mechanical performance, fracture behavior and phonon transport in materials.

The anisotropy factors (A_B, A_G) and the universal anisotropy index (A^U) were determined using the following well-established equations (Ranganathan & Starzewski, 2008; Miao et al., 2011):

$$A_B = \frac{B_V - B_R}{B_V + B_R},\ A_G = \frac{G_V - G_R}{G_V + G_R},\ A^U = 5\frac{G_V}{G_R} + \frac{B_V}{B_R} - 6 \quad (12)$$

where B_V and B_R represent the Voigt and Reuss bulk moduli, respectively, while G_V and G_R denote the corresponding shear moduli, in the case of isotropic materials, these indices are equal to zero, meaning that any deviation from zero is a direct measure of anisotropy (Wei et al.,2021).

The calculated values are presented in Table 4. The percentage bulk modulus anisotropy is relatively low for $Fe_3Al_2B_2$ and $Ru_3Al_2B_2$, indicating that these compounds exhibit nearly isotropic bulk behavior. However, $Os_3Al_2B_2$ shows significantly higher anisotropy, suggesting direction-dependent compressibility. The percentage shear modulus anisotropy values were higher than the percentage bulk modulus values, but the same variation was observed for the compounds. Especially, the anisotropy observed for the percentage shear modulus value of $Os_3Al_2B_2$ compound is remarkable. Moreover, $Os_3Al_2B_2$ exhibits the highest universal anisotropy index (A^U), confirming that it is the most anisotropic among the considered borides. This result is consistent with the significant deviations observed in its elastic properties. In contrast, $Fe_3Al_2B_2$ displays the lowest anisotropy, as evidenced by the relatively small differences between its maximum and minimum elastic moduli, suggesting a more uniform mechanical behavior across different crystallographic directions.

The three-dimensional (3D) elastic property visualizations of the studied compounds were generated using ELATE software (Gaillac et al., 2016) and are presented in Figure 2. It is well established that isotropic materials should exhibit a perfect spherical shape in such 3D representations, while any deviation from spherical is an indication of anisotropic mechanical behavior.

The maximum and minimum values extracted from these 3D plots for Young's modulus, shear modulus, linear compressibility, and Poisson's ratio, which are presented in Table 5. Among the three borides, $Os_3Al_2B_2$ shows the most pronounced anisotropy, with significant deviations in the 3D elastic representations, a large difference between the maximum and minimum Young's modulus values and the Poisson's ratio ν_{min} reaching a negative value. In contrast, $Fe_3Al_2B_2$ appears to be the least anisotropic, as the 3D elastic property plots show only small deviations from a spherical shape, indicating that its mechanical properties are more evenly distributed in different directions. This observation is in agreement with the anisotropy indices and reinforces the idea that $Fe_3Al_2B_2$ has a more uniform mechanical response, making it suitable for applications requiring structural stability under multiaxial loading conditions.

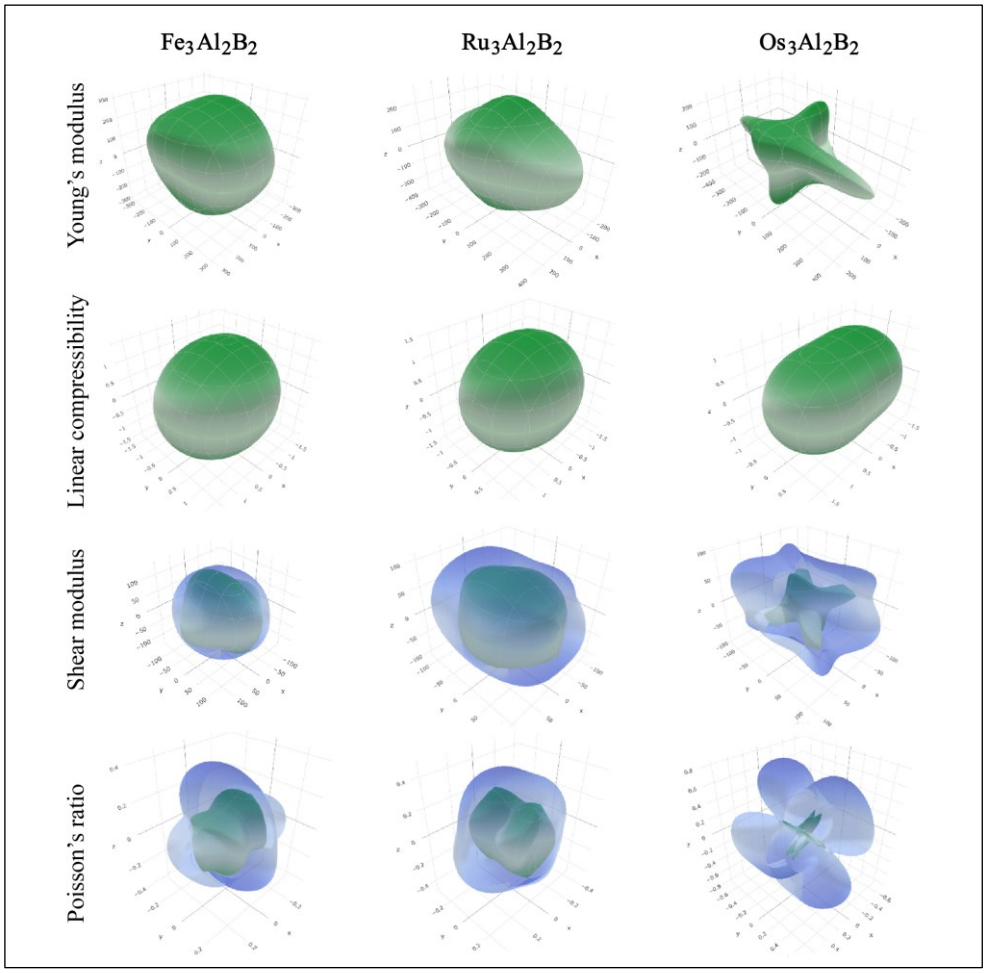

Figure 2. The directional dependence of the mechanical properties for $Fe_3Al_2B_2$, $Ru_3Al_2B_2$, and $Os_3Al_2B_2$ compounds.

Table 5. Maximum and minimum values of Young's modulus (E in GPa), linear compressibility (β in TPa^{-1}), shear moduli (G in GPa), and Poisson's ratio (ν)

Material	E_{max}	E_{min}	β_{max}	β_{min}	G_{max}	G_{min}	ν_{max}	ν_{min}
$Fe_3Al_2B_2$	341.68	240.88	1.765	1.428	136.87	95.52	0.420	0.158
$Ru_3Al_2B_2$	388.75	232.24	1.632	1.301	142.93	84.06	0.496	0.109
$Os_3Al_2B_2$	416.32	85.054	1.765	1.084	146.85	23.82	0.902	-0.064

3.3. Electronic properties

The band structures and partial density of states (PDOS) of the compounds under study have been plotted and presented in Figure 3, using the calculated lattice constants, considering high-symmetry directions and taking Fermi levels as zero.

The band structure shows bands crossing the Fermi level (E_F= 0 eV), indicating the metallic nature of these ternary borides. The relatively flat bands around the Fermi level suggest localized electronic states, while the more dispersed bands indicate good electron mobility, which is important for transport properties. The total DOS at the Fermi level is significant, confirming the presence of conduction electrons. The Fe/Ru/Os-d states dominate near the Fermi level, suggesting that d-orbitals play a crucial role in electrical conductivity. The Al-p and B-p states contribute mainly at lower energy regions, indicating a minor role in electronic conduction.

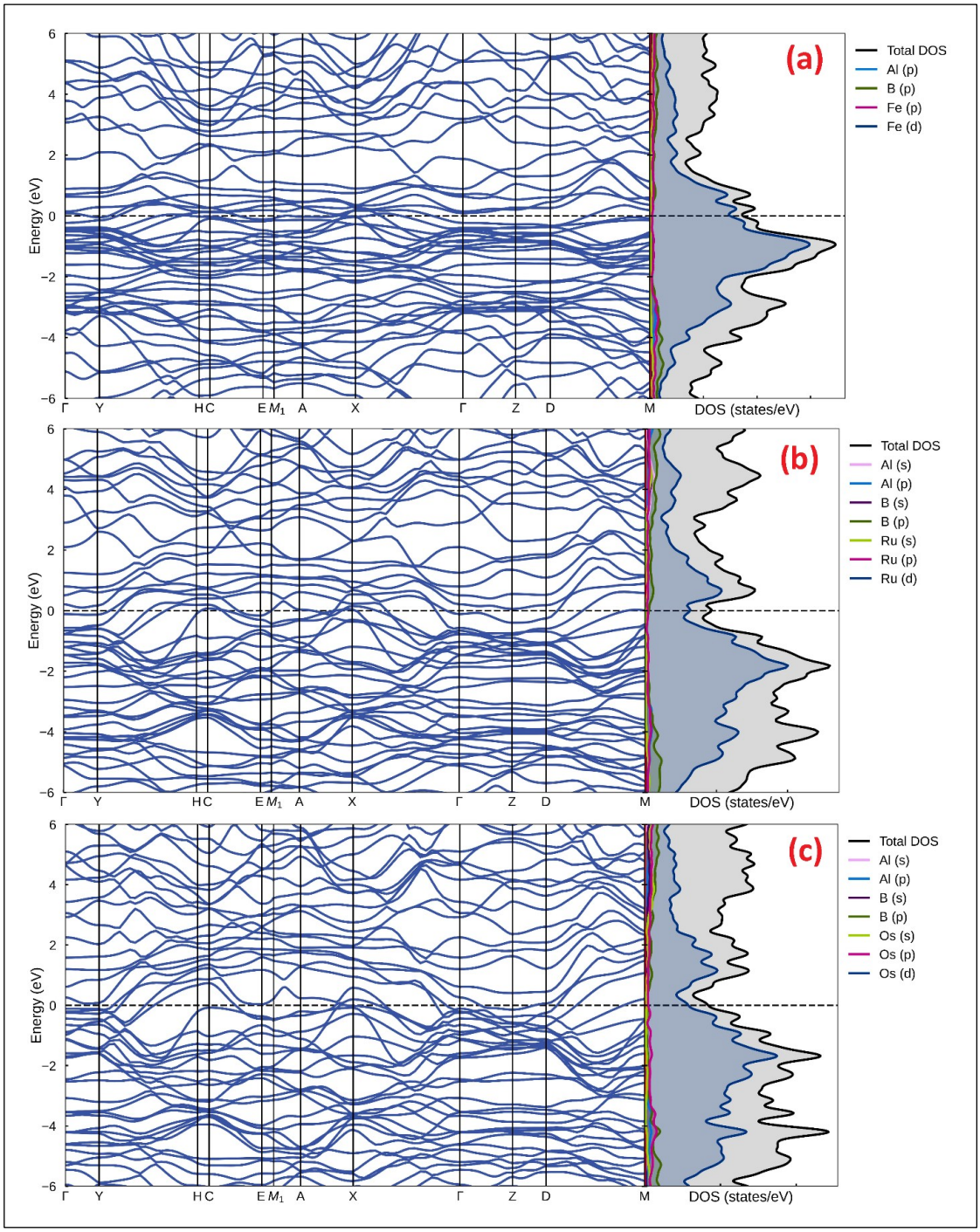

Figure 3. Electronic band structures and density of states; (a) $Fe_3Al_2B_2$, (b) $Ru_3Al_2B_2$, (c) $Os_3Al_2B_2$.

3.4. Vibrational properties

Phonon analysis is important for understanding the dynamic stability of the material, its thermal properties and lattice vibrations. The obtained phonon dispersion curves and phonon density of states shown in Figure 4. No imaginary frequencies are observed in the phonon dispersion, confirming that $Fe_3Al_2B_2$ and $Ru_3Al_2B_2$ are dynamically stable at equilibrium conditions. The phonon dispersion of $Os_3Al_2B_2$ revealed negative vibrational modes around E-M_1 and X. While the highest optical mode is separated from the other optical modes for all compounds, a phonon gap between 10-15 THz was observed for $Fe_3Al_2B_2$, indicating a separation between different vibrational modes that may affect the thermal transport properties.

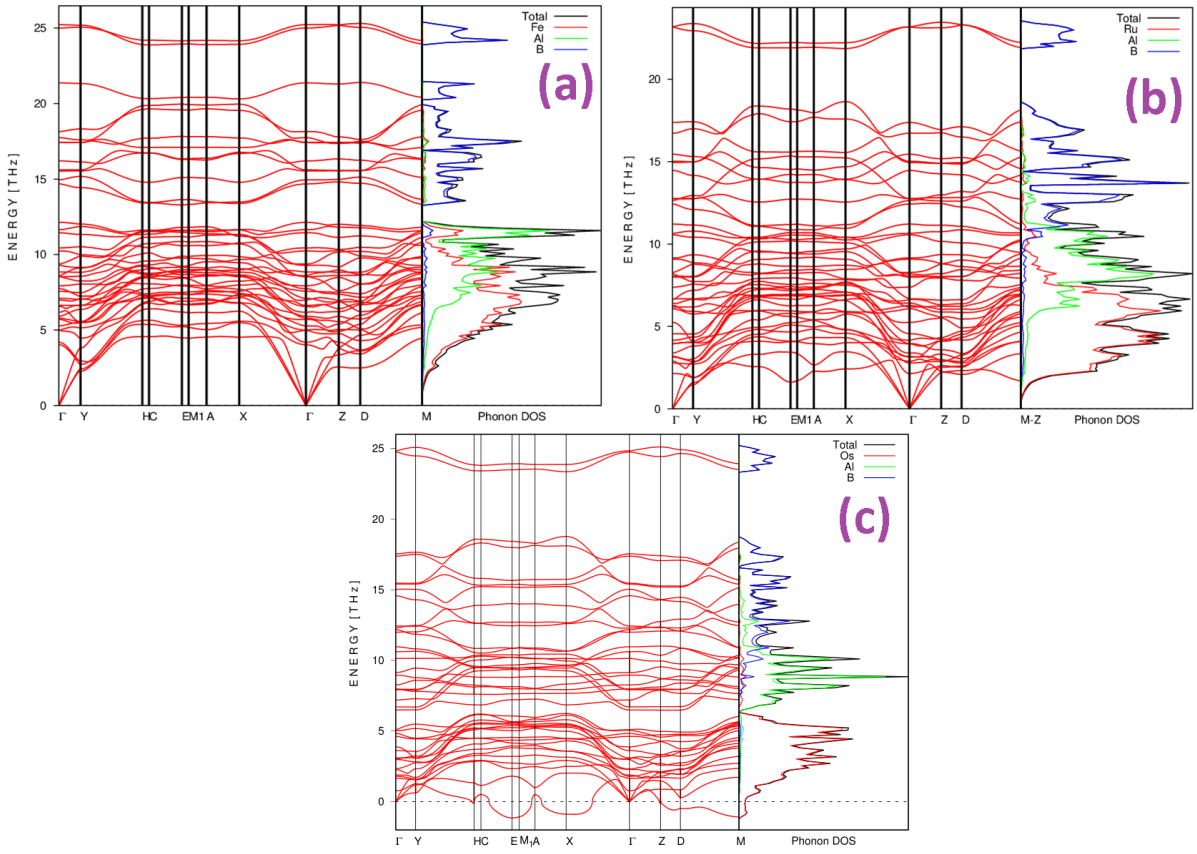

Figure 4. Phonon dispersion curves and phonon density of states; (a) $Fe_3Al_2B_2$, (b) $Ru_3Al_2B_2$, and (c) $Os_3Al_2B_2$.

The acoustic branches of $Fe_3Al_2B_2$ and $Ru_3Al_2B_2$ were dominated by the vibrations of Fe/Ru, while the lower optical branches were dominated by the vibrations of Fe/Ru and Al, and the middle and upper optical branches were dominated by the vibrations of B.

3.5. Thermodynamic properties

The temperature dependence of the free energy (F), entropy (S) and heat capacity (C_v) at constant volume for each boride is given using the equations given in Ref. (Ozisik et al., 2013) and calculated with the data obtained from VASP and Phonopy codes. The Figure 5 presents the thermodynamic properties of $Fe_3Al_2B_2$, $Ru_3Al_2B_2$, and $Os_3Al_2B_2$ as a function of temperature, including Helmholtz free energy (F), entropy (S) and heat capacity (C_v). These properties are essential for understanding the thermal stability of the material and its behavior at different temperatures.

The temperature variation of the thermodynamic functions exhibits a similar trend for the considered ternary borides. It is known that below Debye temperature is defined as low temperature for solids. The decrease in free energy is gradual at low temperatures, but at higher temperatures the slope becomes more pronounced. The free energy decreases with increasing temperature, which is a typical behavior for stable materials. Negative values at high temperatures indicate thermodynamic stability, indicating that these borides remain energetically favorable over a wide temperature range. Entropy (S) increases with temperature due to the increasing disorder in the system. As expected, the entropy increases monotonically with temperature, because increasing temperature leads to more atomic disorder. At low temperatures, the entropy increases (Ozisik et al., 2011), which is typical for solid-state materials due to the increased vibrational contributions of phonons. At high temperatures, the entropy increase slows down, indicating that the system is approaching a value at which the phonon contributions reach maximum efficiency. At low temperatures, the heat capacity follows a T^3 dependence consistent with the Debye model, where phonon vibrations are the dominant contributor. At high temperatures, the

heat capacity approaches a nearly constant value, consistent with the Dulong-Petit limit, which states that the heat capacity of solids tends towards a constant value at high temperatures.

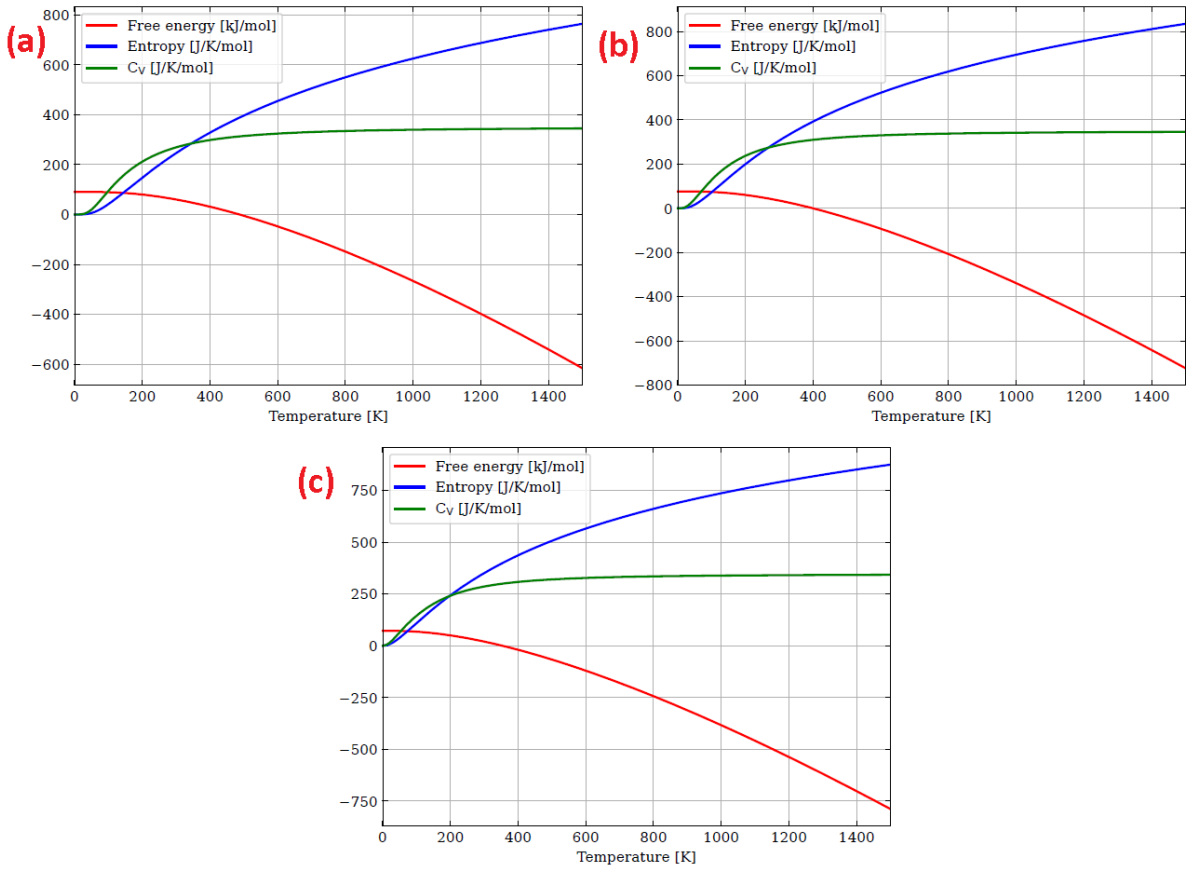

Figure 5. The calculated free energy, entropy, and heat capacity; (a) $Fe_3Al_2B_2$, (b) $Ru_3Al_2B_2$, and (c) $Os_3Al_2B_2$.

4. Conclusion

In this study, the structural, mechanical, electronic, vibrational and thermal properties of $Fe_3Al_2B_2$, $Ru_3Al_2B_2$, and $Os_3Al_2B_2$ were investigated using first-principles calculations based on density functional theory. The results show that all compounds are thermodynamically stable and $Fe_3Al_2B_2$ exhibits the highest structural stability as indicated by the lowest formation energy. Mechanical analysis reveals that $Os_3Al_2B_2$ has the highest bulk modulus with strong resistance to volume deformation, while $Fe_3Al_2B_2$ shows the highest shear modulus, making it the most resistant to shear-induced deformations. Furthermore, elastic anisotropy calculations show that $Os_3Al_2B_2$ exhibits the highest degree of anisotropy among the studied borides, while $Fe_3Al_2B_2$ exhibits a more isotropic structure and provides a more uniform mechanical response along different crystallographic directions. Electronic structure calculations confirm the metallic nature of all three compounds. The phonon dispersion analysis suggests that $Fe_3Al_2B_2$ and $Ru_3Al_2B_2$ are dynamically stable, while $Os_3Al_2B_2$ exhibits negative phonon modes, indicating potential vibrational instability. The thermodynamic analysis confirms the thermal stability of these borides, with free energy consistently decreasing and entropy increasing as temperature rises. The heat capacity trends suggest that $Fe_3Al_2B_2$, $Ru_3Al_2B_2$ and $Os_3Al_2B_2$ follow conventional solid-state behavior, making it a promising candidate for high-temperature applications. $Fe_3Al_2B_2$ appears to be the most promising compound in terms of mechanical strength and thermal stability, making it a strong candidate for applications requiring high structural stability. On the other hand, $Os_3Al_2B_2$, with its remarkable anisotropic properties, may be particularly suitable for applications requiring direction-dependent mechanical behavior.

Acknowledgements

The numerical calculations reported in this study were fully performed at TUBITAK ULAKBIM, High Performance and Grid Computing Center (TRUBA resources).

References

Ade, M., & Hillebrecht, H. (2015). Ternary borides Cr_2AlB_2, Cr_3AlB_4, and Cr_4AlB_6: The first members of the series $(CrB_2)_nCrAl$ with n = 1, 2, 3 and a unifying concept for ternary borides as MAB-phases. *Inorganic Chemistry, 54*(13), 6122–6135. https://doi.org/10.1021/acs.inorgchem.5b00049

Ali, M. A., Hadi, M. A., Hossain, M. M., Naqib, S. H., & Islam, A. K. M. A. (2017). Theoretical investigation of structural, elastic, and electronic properties of ternary boride MoAlB. *Physica Status Solidi B, 254*(7), 1700010. https://doi.org/10.1002/pssb.201700010

Ali, M. M., Hadi, M. A., Rahman, M. L., Haque, F. H., Haider, A. F. M. Y., & Aftabuzzaman, M. (2020). DFT investigations into the physical properties of a MAB phase Cr_4AlB_4. *Journal of Alloys and Compounds, 821*, 153547. https://doi.org/10.1016/j.jallcom.2019.153547

Anderson, O. L. (1963). A simplified method for calculating the Debye temperature from elastic constants. *Journal of Physics and Chemistry of Solids, 24*(7), 909–917. https://doi.org/10.1016/0022-3697(63)90067-2

Blum, Y. D., Marschall, J., Hui, D., & Young, S. (2008). Thick protective UHTC coatings for SiC-based structures: Process establishment. *Journal of the American Ceramic Society, 91*(5), 1453–1460. https://doi.org/10.1111/j.1551-2916.2008.02360.x

Cheng, Y., Lv, Z. L., Chen, X. R., & Cai, L. C. (2014). Structural, electronic and elastic properties of $AlFe_2B_2$: First-principles study. *Computational Materials Science, 92*, 253–257. https://doi.org/10.1016/j.commatsci.2014.05.048

Corral, E. L., & Loehman, R. E. (2008). Ultra-high temperature ceramic coatings for oxidation protection of carbon-carbon composites. *Journal of the American Ceramic Society, 91*(5), 1495–1502. https://doi.org/10.1111/j.1551-2916.2008.02331.x

Eremets, M. I., Struzhkin, V. V., Mao, H. K., & Hemley, R. J. (2001). Superconductivity in boron. *Science, 293*(5528), 272–274. https://doi.org/10.1126/science.1062286

Eroğlu, E., Toffoli, H., Mutlu, R. N., Kandasamy, J., Karaca, M., & Gökalp, I. (2023). Exploring the interaction of water with boron surfaces using density functional theory. *Journal of Boron*, 8(1), 25–31. https://doi.org/10.30728/boron.1283831

Fahrenholtz, W. G., Hilmas, G. E., Talmy, I. G., & Zaykoski, J. A. (2007). Refractory diborides of zirconium and hafnium. *Journal of the American Ceramic Society, 90*(5), 1347–1364. https://doi.org/10.1111/j.1551-2916.2007.01583.x

Feng, S., Yang, Y., Chen, P., Tang, C., & Cheng, X. (2018). A first-principles study of hypothetical Ti_4AlB_3 and V_4AlB_3 phases. *Solid State Communications, 281*, 17–21. https://doi.org/10.1016/j.ssc.2018.06.009

Gaillac, R., Cudazzo, P., & Rignanese, G. M. (2016). ELATE: A software to visualize and analyze the elastic tensors. *Journal of Physics: Condensed Matter, 28*(27), 275201. https://doi.org/10.1088/0953-8984/28/27/275201

Herbst, J. F., Fuerst, C. D., & Mishira, R. K. (1991). Coercivity enhancement of melt-spun Nd–Fe–B ribbons using low-level Cu additions. *Journal of Applied Physics, 69*(8), 5823–5825. https://doi.org/10.1063/1.347861

Hill, R. (1952). The elastic behaviour of a crystalline aggregate. *Proceedings of the Physical Society. Section A, 65*(5), 349–354. https://doi.org/10.1088/0370-1298/65/5/307

Hirt, S., Hilfinger, F., & Hillebrecht, H. (2018). Synthesis and crystal structures of the new ternary borides $Fe_3Al_2B_2$ and $Ru_9Al_3B_8$ and the confirmation of $Ru_4Al_3B_2$ and $Ru_9Al_5B_{8-x}$ (x≈2). *Zeitschrift für Kristallographie - Crystalline Materials, 233*(5), 295–307. https://doi.org/10.1515/zkri-2017-2095

Huang, Q., Lin, Q., Xu, Y., & Cao, Y. (2025). Predicting potential hard materials in Nb–B ternary boride: First-principles calculations. *International Journal of Refractory Metals and Hard Materials, 126*, 106927. https://doi.org/10.1016/j.ijrmhm.2024.106927

Johnston, I., Keeler, G., Rollins, R., & Spicklemine, S. (1996). *The consortium for upper-level physics software: Solid State Physics Simulations*. New York: John Wiley & Sons.

Kota, S., Wang, W., Lu, J., Natu, V., Opagiste, C., Ying, G., Hultman, L., May, S. J., & Barsoum, M. W. (2018). Magnetic properties of Cr_2AlB_2, Cr_3AlB_4, and CrB powders. *Journal of Alloys and Compounds, 767*, 474–482. https://doi.org/10.1016/j.jallcom.2018.07.031

Kresse, G., & Furthmüller, J. (1996a). Efficiency of ab-initio total energy calculations for metals and semiconductors using a plane-wave basis set. *Computational Materials Science, 6*(1), 15–50. https://doi.org/10.1016/0927-0256(96)00008-0

Kresse, G., & Furthmüller, J. (1996b). Efficient iterative schemes for ab initio total energy calculations using a plane-wave basis set. *Physical Review B, 54*(16), 11169–11186. https://doi.org/10.1103/PhysRevB.54.11169

Kresse, G., & Joubert, D. (1999). From ultrasoft pseudopotentials to the projector-augmented-wave method. *Physical Review B, 59*(3), 1758–1775. https://doi.org/10.1103/PhysRevB.59.1758

Le Page, Y., & Saxe, P. (2002). Symmetry-general least-squares extraction of elastic data for strained materials from ab initio calculations of stress. *Physical Review B, 65*(10), 104104. https://doi.org/10.1103/PhysRevB.65.104104

Licht, S., Yu, X. W., & Qu, D. Y. (2007). A novel alkaline redox couple: Chemistry of the Fe^{6+}/B^{2-} super-iron boride battery. *Chemical Communications, 2007*(26), 2753–2755. http://dx.doi.org/10.1039/b701629h

Lu, J., Kota, S., Barsoum, M. W., & Hultman, L. (2017). Atomic structure and lattice defects in nanolaminated ternary transition metal borides. *Materials Research Letters, 5*(4), 235–241. https://doi.org/10.1080/21663831.2016.1245682

Martini, C., Palombarini, G., Poli, G., & Prandstraller, D. (2004). Sliding and abrasive wear behaviour of boride coatings. *Wear, 256*(6), 608–613. https://doi.org/10.1016/j.wear.2003.10.003

Miao, N., Sa, B., Zhou, J., & Sun, Z. (2011). Theoretical investigation on the transition-metal borides with Ta_3B_4-type structure: A class of hard and refractory materials. *Computational Materials Science, 50*(4), 1559-1566. https://doi.org/10.1016/j.commatsci.2010.12.015

Monkhorst, H. J., & Pack, J. D. (1976). Special points for Brillouin-zone integrations. *Physical Review B, 13(12)*, 5188-5192. https://doi.org/10.1103/PhysRevB.13.5390

Mouhat, F., & Coudert, F. X. (2014). Necessary and sufficient elastic stability conditions in various crystal systems. *Physical Review B, 90*(22), 224104. https://doi.org/10.1103/PhysRevB.90.224104

Opeka, M. M., Talmy, I. G., Wuchina, E. J., Zaykoski, J. A., & Causey, S. J. (1999). Mechanical, thermal, and oxidation properties of refractory hafnium and zirconium compounds. *Journal of the European Ceramic Society, 19*(13–14), 2405–2414. https://doi.org/10.1016/S0955-2219(99)00129-6

Ozisik, H., Colakoglu, K., Ozisik, H. B., & Deligoz, E. (2010). Structural, elastic, and lattice dynamical properties of Germanium diiodide (GeI_2). *Computational Materials Science, 50*(2), 349–355. http://dx.doi.org/10.1016/j.commatsci.2010.08.026

Ozisik, H., Colakoglu, K., Deligoz, E., & Ateser, E. (2013). First-principles calculations of vibrational and thermodynamical properties of rare-earth diborides. *Computational Materials Science, 68*, 307–313. http://dx.doi.org/10.1016/j.commatsci.2012.11.003

Ozisik, H., Deligoz, E., Colakoglu, K., & Ciftci, Y. O. (2011). Structural, elastic, and lattice dynamical properties of YB_2 compound. *Computational Materials Science, 50*(3), 1057–1063. http://dx.doi.org/10.1016/j.commatsci.2010.10.046

Ozisik, H., Deligoz, E., Surucu, G., & Ozisik, H. B. (2016). Anisotropic elastic and vibrational properties of Ru_2B_3 and Os_2B_3: A first-principles investigation. *Materials Research Express, 3*(7), 076501. http://dx.doi.org/10.1088/2053-1591/3/7/076501

Panda, K. B., & Chandran, K. S. R. (2006). First-principles determination of elastic constants and chemical bonding of titanium boride (TiB). *Acta Materialia, 54*(6), 1641–1657. https://doi.org/10.1016/j.actamat.2005.12.003

Perdew, J. P., Burke, K., & Ernzerhof, M. (1996). Generalized gradient approximation made simple. *Physical Review Letters, 77*(18), 3865–3868. https://doi.org/10.1103/PhysRevLett.77.3865

Pugh, S. F. (1954). Relations between the elastic moduli and the plastic properties of polycrystalline pure metals. *Philosophical Magazine, 45*(367), 823–843. https://doi.org/10.1080/14786440808520496

Ranganathan, S. I., & Starzewski, M. O. (2008). Elastic properties of nanoscale materials. *Physical Review Letters, 101*(5), 055504. https://doi.org/10.1103/PhysRevLett.101.055504

Reuss, A. (1929). Berechnung der Fließgrenze von Mischkristallen auf Grund der Plastizitätsbedingung für Einkristalle. *ZAMM - Zeitschrift für Angewandte Mathematik und Mechanik, 9*(1), 49–58. https://doi.org/10.1002/zamm.19290090104

Schreiber, E., Anderson, O. L., Soga, N., & Bell, J. F. (1975). *Elastic constants and their measurement*. New York: McGraw-Hill.

Takagi, K. (2006). Development and application of high-strength ternary boride-based cermets. *Journal of Solid-State Chemistry, 179*(9), 2809–2818. https://doi.org/10.1016/j.jssc.2006.01.023

Togo, A. (2023). First-principles phonon calculations with Phonopy and Phono3py. *Journal of the Physical Society of Japan, 92*(1), 012001. https://doi.org/10.7566/JPSJ.92.012001

Togo, A., Chaput, L., Tadano, T., & Tanaka, I. (2023). Implementation strategies in phonopy and phono3py. *Journal of Physics: Condensed Matter*, *35*(35), 353001. https://iopscience.iop.org/article/10.1088/1361-648X/acd831/meta

Voigt, W. (1966). *Lehrbuch der Kristallphysik*. Wiesbaden: Vieweg+Teubner Verlag.

Wei, J., Zhang, L., & Liu, Y. (2021). First-principles calculations of mechanical and thermal properties of Cr–Al–B ternary borides. *Solid State Communications, 326*, 114182. https://doi.org/10.1016/j.ssc.2020.114182

Yu, X. W., & Licht, S. (2008). A novel high-capacity, environmentally benign energy storage system: Super-iron boride battery. *Journal of Power Sources, 179*(1), 407–411. https://doi.org/10.1016/j.jpowsour.2007.12.060

Zapata-Solvas, E., Jayaseelan, D. D., Brown, P. M., & Lee, W. E. (2013). Thermal properties of La_2O_3-doped ZrB_2- and HfB_2-based ultra-high temperature ceramics. *Journal of the European Ceramic Society, 33*(15–16), 3467–3472. https://doi.org/10.1016/j.jeurceramsoc.2013.06.009

Zhang, H., Dai, F., Xiang, H., Wang, X., Zhang, Z., & Zhou, Y. (2019a). Phase pure and well-crystalline Cr_2AlB_2: A key precursor for two-dimensional CrB. *Journal of Materials Science & Technology, 35*(8), 1593–1600. https://doi.org/10.1016/j.jmst.2019.03.031

Zhang, H., Dai, F., Xiang, H., Zhang, Z., & Zhou, Y. (2019b). Crystal structure of Cr_4AlB_4: A new MAB phase compound discovered in the Cr-Al-B system. *Journal of Materials Science & Technology, 35*(4), 530–534. https://doi.org/10.1016/j.jmst.2018.10.006

Zhang, H., Xiang, H., Dai, F., Zhang, Z., & Zhou, Y. (2018). First demonstration of possible two-dimensional MBene CrB derived from MAB phase Cr_2AlB_2. *Journal of Materials Science & Technology, 34*(11), 2022–2026. https://doi.org/10.1016/j.jmst.2018.02.024